



HHS Public Access

Author manuscript

Inhal Toxicol. Author manuscript; available in PMC 2017 December 05.

Published in final edited form as:

Inhal Toxicol. 2016 December ; 28(14): 686–697. doi:10.1080/08958378.2016.1257664.

Role of engineered metal oxide nanoparticle agglomeration in reactive oxygen species generation and cathepsin B release in NLRP3 inflammasome activation and pulmonary toxicity

Tina M. Sager^{1,2}, Michael Wolfarth², Stephen S. Leonard², Anna M. Morris², Dale W. Porter², Vincent Castranova^{2,3}, and Andrij Holian¹

¹Center for Environmental Health Sciences, University of Montana, Missoula, MT

²National Institute for Occupational Safety and Health, Health Effects Laboratory Division, Pathology and Physiology Research Branch, Morgantown, WV

³Department of Pharmaceutical Sciences, West Virginia University School of Pharmacy, Morgantown, WV

Abstract

Incomplete understanding of the contributions of dispersants and engineered nanomaterial (ENM) agglomeration state to biological outcomes presents an obstacle for toxicological studies. Although reactive oxygen species (ROS) production is often regarded as the primary indicator of ENM bioactivity and toxicity, it remains unclear whether ENM produce ROS or whether ROS is an outcome of ENM-induced cell injury. Phagolysosomal disruption and cathepsin B release also promotes bioactivity through inflammasome activation. Therefore, specific particle parameters, i.e. pre-exposure dispersion status and particle surface area, of two ENM (NiO and CeO₂) were used to evaluate the role of ROS generation and cathepsin B release during ENM-induced toxicity. Male C57BL/6J mice were exposed to 0, 20, 40, or 80 µg of poorly- or well-dispersed NiO-NP or CeO₂-NP in four types of dispersion media. At 1 and 7 days post-exposure, lung lavage fluid was collected to assess inflammation, cytotoxicity, and inflammasome activation. Results showed that pre-exposure dispersion status correlated with post-exposure pulmonary bioactivity. The differences in bioactivity of NiO-NP and CeO₂-NP are likely due to NiO-NP facilitating the release of cathepsin B and in turn inflammasome activation generating pro-inflammatory cytokines. Further, both metal oxides acted as free radical scavengers. Depending on the pH, CeO₂-NP acted as a free radical scavenger in an acidic environment (an environment mimicking the lysosome) while the NiO-NP acted as a scavenger in a physiological pH (an environment that

Please address all correspondence to: Dr. Tina M. Sager, National Institute for Occupational Safety and Health, 1095 Willowdale Road, Morgantown WV 26505. (T) 304-285-6109 (F) 304-285-5938 (E) sst2@cdc.gov.

Competing interests

The authors declare that they have no competing interests.

Authors' contributions

TMS and MW carried out all of the *in vivo* experiments involved in this study including the pharyngeal aspirations and animal sacrifices. TMS drafted the MS and performed statistical analysis. TMS, VC, and AH conceived of the study and participated in its design. SL and AM carried out the ESR particle analysis. TMS, VC, DWP, and AH participated in the study coordination, data analysis and interpretation, and helped draft the MS. All authors read and approved the final MS.

mimics the cytosol of the cell). Therefore, results from this study suggest that ENM-induced ROS is not likely a mechanism of inflammasome activation.

Keywords

Pulmonary toxicity; engineered nanoparticles; ROS; agglomeration; inflammasome; activation; inflammation; cytotoxicity

Background

Engineered nanoparticles/materials (ENM) are now being incorporated into a multitude of different products. The unique physiochemical properties of ENM support their wide variety of applications. However, the unique physiochemical properties of ENM introduce a wide range of concerns pertaining to human health (Shvedova et al. 2012; Manke et al. 2013). One of the challenges in evaluating potential adverse effects of ENM is due to their unique and extensive tendency to agglomerate and the lack of a uniform set of guidelines to prepare ENM suspensions for *in vitro* or *in vivo* studies. In order to develop procedures to evaluate potential ENM hazards, studies elucidating the roles of dispersion media and agglomerate size on bioactivity as well as the mechanisms facilitating bioactivity need to be undertaken to understand the roles of these factors to reduce experimental variability.

Numerous studies on size- and shape-dependent toxicity of nanoparticles have demonstrated the biological importance of these properties (Chithrani et al. 2006; Powers et al. 2007; Lewinski et al. 2008; Murphy et al. 2008; Wang et al. 2008). These parameters affect cellular uptake, protein adsorption, accumulation in organelles and distribution throughout the body. One reason for these effects is the correlation between particle size and surface area. In general, for a fixed mass of particles, surface area increases as particle size becomes smaller. Thus, particle surface area may explain the greater toxicity of nanoparticles compared with an equal mass of fine particles of the same material (Donaldson et al. 2002; Monteiller et al. 2007; Sager et al. 2009). Since it is the surface atoms and molecules that play a significant role in determining the bulk properties of the nanoparticle, most of the previous toxicity studies have demonstrated an inverse relationship between particle size and toxicity.

However, agglomeration of nanoparticles can dramatically change the original size and shape of the particles when delivered to biological models *in vitro* or *in vivo* (Sager et al. 2016). Nanoparticles tend to easily agglomerate due to their high surface energy, but can be partially dispersed by sonication when loosely bound. Agglomeration alters the size and shape of nano-particles within the suspension; this, in turn, greatly influences the cell-particle interactions. A lack of understanding of the contributions of dispersants and agglomeration state to biological effects hinders the study of the actual effects of particle size and shape on toxicity (Sager et al. 2007; Wang et al. 2008; Auffan et al. 2010; Keller et al. 2010).

Some of the paradigms for ENM-mediated toxicity include oxidative stress, inflammation, genetic damage, and the inhibition of cell division and cell death (Stone et al. 2007; Ju-Nam

and Lead 2008; Li et al. 2008; Johnston et al. 2010). Most work to date has suggested that ROS generation and consequent oxidative stress are frequently observed with ENM toxicity (Li et al. 2010 ; Shvedova et al., 2012). However, it may be inaccurate to assume that ROS generation is a prerequisite to NP-induced toxicity since a few studies have reported the direct toxicity of NP without causing ROS (Wang et al. 2010). Nevertheless, ROS generation may be a major event during NP-induced injury that needs to be thoroughly characterized in order to predict NP-induced toxicity.

Current evidence also suggests that toxic nanoparticles could potentially increase phagolysosomal membrane permeability and release of cathepsin B which also promotes the activation of the NLRP3 inflammasome. Cathepsin B release, in turn, induces release of pro-inflammatory cytokines (IL-1 β and IL-18) from alveolar macrophages (AM) (Beamer et al. 2012). It was previously shown that the NLRP3 inflammasome is activated *in vivo*, after pulmonary exposure to MWCNT (Sager et al. 2014). Studies have concluded that upon assembly of the intact NLRP3 inflammasome, caspase-1 becomes activated and produces the mature and secreted forms of the pro-inflammatory cytokines interleukin IL-1 β and IL-18 (Jin and Flavell, 2010). The NLRP3 inflammasome activation pathway model uptake of nanoparticles causes the disruption of the phagolysosome acidic compartment and subsequent release of cathepsin B; inhibition of this process has been proven to block the inflammasome activation.

To date, an exploration into the cellular mechanisms driving inflammasome activation by nanoparticle induced pulmonary injury, whether it be ROS generation or cathepsin B release, is incomplete and remains to be fully elucidated. Therefore, the current study evaluated specific particle parameters, i.e. pre-exposure dispersion status and particle surface area, of two highly utilized metal oxides to evaluate the role of ROS generation and inflammasome activation during ENM-induced toxicity.

NiO was chosen as one particle for these experiments due to the fact that previous studies have reported that NiO nanoparticles stimulate pulmonary bioactivity (Gillespie et al. 2010; Horie et al. 2011; Sager et al. 2016). CeO₂ was chosen as a comparison particle due to the evidence that it is a nanoparticle that can display either a beneficial (anti-oxidant) or toxic (oxidant) effect (Asati et al. 2010) in differing experimental situations. The purpose of this study was not to compare the bioactivity of CeO₂ to NiO, as both particles have been shown to facilitate pulmonary inflammation and pathology in certain experimental situations, but instead to explore and assess how parameters, like pre-exposure dispersion and ROS production, and inflammasome activation may facilitate the differences between the pulmonary toxicity of these two metal oxides.

Materials and Methods

Particles and characterization

CeO₂-nanoparticles (CeO₂-NP) were obtained from Sigma (cerium (IV) oxide; < 25 nm; Cat. #544841; St. Louis, MO). Nickel oxide nanoparticles (NiO-NP) were also obtained from Sigma (nickel II oxide nanopowder; Cat. #637130). Both NiO- and CeO₂-NP were separately suspended in one of four different, commonly utilized dispersion medias:

phosphate buffered saline (PBS), dispersion media (DM; combination of dipalmitoyl-phosphatidyl choline (DPPC) and albumin in concentrations that mimic diluted alveolar lining fluid) (Porter et al. 2008) and two commercially available surfactants; Survanta® and pluronics (pluronics F-68). Both well-dispersed (20 min sonication) and poorly-dispersed (5 min sonication) suspensions were produced utilizing both CeO₂-NP and NiO-NP in each media. Each particle suspension (1.6 mg/ml) was sonicated utilizing a Branson Sonifer 450 (Branson Ultrasonics Corp., Danbury, CT) at 25W continuous output for 20 min or for 5 min to generate well-dispersed or poorly-dispersed suspensions, respectively. During sonication, heat was dissipated by placing the samples on ice.

After the particle suspensions were prepared as described above, 2-ml samples were immediately transferred to a cuvette and particle size range was immediately determined by dynamic light scattering (DLS). For each NP/suspension media combination, DLS analysis was conducted 10 separate times on 10 different samples. The 10 individual run results were then utilized to calculate the average hydrodynamic diameter for each sample analyzed. DLS analysis for each sample was conducted using a Nanotracer 252 (Microtrac; Montgomeryville, PA).

Electron microscopy (EM) analyses were also conducted on the same samples. For the EM analysis, each particle suspension was diluted in diH₂O 1:1000 to prevent salt and protein components of the dispersion solutions from creating artifacts and preventing accurate interpretation. Next, a 0.5 ml sample of each suspension was then filtered through a 0.2- μ m Nucleopore filter onto a Formvar-coated copper grid to dry. Each sample was then imaged using a Hitachi field emission scanning electron microscope (FESEM).

The surface charge of each nanoparticle/suspension media combination was also analyzed using a Malvern Zetasizer Nano ZS instrument (Malvern Instruments Inc., Malvern, UK). Each zeta potential measurement represents the arithmetic mean of 10 individual measurements made by the instrument for each NP/suspension media combination. The electrophoretic mobility of both NiO-NP and CeO₂-NP in each media was converted into the zeta potential by utilizing the Helmholtz-Smoluchowski equation. The surface area of both the NiO-NP and the CeO₂-NP were also measured by the Brunauer-Emmett-Teller (BET) method. BET measurements were taken on each particle sample in its dry state under N₂ adsorption to measure specific surface area (Brunauer et al. 1938).

Electron Spin Resonance (ESR) Measurements

Xanthine, xanthine oxidase and 5-5-dimethyl-1-pyrroline-oxide (DMPO) were purchased from Sigma. The spin trap, DMPO, was purified by charcoal de-colorization and vacuum distillation and was free of electron spin resonance (ESR) detectable impurities.

Free radical measurements—ESR and spin trapping were used to detect short-lived free radical intermediates. Radicals were measured using the addition-type reaction of a short-lived radical with a compound (spin trap) to form a relatively long-lived paramagnetic free radical product (spin adduct), which could then be studied using conventional ESR measurements. Concentrations given in the figure legends are final concentrations.

The intensity of the signal was used to measure the relative amount of short-lived radicals trapped, and the hyperfine couplings of the spin adduct are characteristic of the original trapped radicals. Spin trapping is the method of choice for detection and identification of free radical generation because of its specificity and sensitivity. All ESR measurements were conducted using a Bruker EMX spectrometer (Bruker Instruments, Billerica, MA) and a flat cell assembly. Hyperfine couplings were measured (to 0.1 G) directly from magnetic field separation using potassium tetra-peroxochromate (K_3CrO_8) and 1,1-diphenyl-2-picrylhydrazyl as reference standards. The relative radical concentration was estimated by multiplying half of the peak height by $(\Delta H_{pp})^2$, where ΔH_{pp} represents peak-to-peak width. Acquisit (Bruker) was used for data acquisitions and analyses.

Reaction system—The free radical spin trap system was composed of DMPO (100 mM), particle (CeO_2 , NiO) xanthine (35 mM) and xanthine oxidase (4 μ l/ml). Measurements were conducted in artificial lysosome fluid (ALF), a fluid which mimics the acidic environment inside a lysosome, and DM, which mimics the neutral pH in the cell cytosol. ALF was prepared as described in Marques et al (2011). The reaction was allowed to incubate for 3 min at room temperature. ESR settings are given in figure legends.

Animals

C57BL/6J mice (male, 7-wk-old) were purchased from the Jackson Laboratories (Bar Harbor, ME). Mice were housed in an AAALAC-accredited, specific-pathogen-free, environment-controlled facility and allowed to acclimate at least 7 days prior to use. The mice were monitored to be free of endogenous viral pathogens, parasites, mycoplasmas, *Helicobacter*, and *CAR Bacillus*. Mice were kept in ventilated cages, that were provided HEPA-filtered air and both Diamond-Dry virgin cellulose and hardwood Sani-chips for bedding. The mice were maintained on a Harlan Teklad 7913, 6% fat, irradiated diet and tap water, both of which were available *ad libitum*. All experimental procedures were approved by the Animal Care and Use Committee of the University of Montana prior to beginning the study.

Mouse pharyngeal aspiration

Mice were exposed to 0, 20, 40, or 80 μ g/mouse of a poorly- or well-dispersed NiO-NP or CeO_2 -NP/suspension media combination via pharyngeal aspiration. For pharyngeal aspiration, a stock solution of each CeO_2 -NP and NiO-NP/suspension media combination (1.6 mg/ml) (well-dispersed and poorly-dispersed) was prepared utilizing the previously described sonication parameters (5 min vs. 20 min, 25W, and continuous output). From the prepared stock solution of each NP/suspension media combination dilutions were made to produce final NP concentrations of 20, 40, or 80 μ g/mouse. Immediately upon preparation of each CeO_2 -NP or NiO-NP/suspension media combination, pharyngeal aspiration was conducted as described by Rao et al. (2003). In brief, the animals were anesthetized with isoflurane and placed on a board in a near vertical position. The tongue was extended with lined forceps; 50 μ l respective particle suspension was placed on the back of the tongue which was held until the suspension was aspirated. Control mice were administered an equal volume of the dispersion media being utilized.

Collection of lung lavage fluid

At 1 and 7 day post-exposure, mice were euthanized by intraperitoneal (IP) injection of sodium pentobarbital (100–300 mg/kg body weight) followed by exsanguination. The trachea was cannulated with a blunt 22-G needle and whole lung lavage (WLL) was performed using cold sterile Ca^{+2} , Mg^{+2} -free PBS at a volume of 0.6 ml for first lavage (kept separate) and 1 ml for subsequent lavages. Approximately 4 ml WLL fluid/mouse was collected in sterile centrifuge tubes. Collected WLL cells were washed in PBS by centrifugation ($600 \times g$, 5 min, 4°C) and re-suspended in PBS (Zeidler et al. 2004). Acellular first-fraction WLL aliquots were frozen or kept on ice for analysis.

Cell counts and differentials and WLL fluid analyses

Total WLL cell counts were obtained using a Coulter Multisizer 3 (Coulter Electronics, Hialeah, FL) and cytospin preparations of the cells were made using a cytocentrifuge (Shandon, London, UK). The preparations were stained with modified Wright-Giemsa stain and differentials determined by light microscopy. Lactate dehydrogenase (LDH) activity of the first WLL fluid was measured [to assess cytotoxicity] using a COBAS MIRA Plus chemical analyzer (Roche Diagnostics, Montclair, NJ) as previously described (Porter et al. 2002).

The presence of inflammatory mediators (cathepsin B, IL-1 β and IL-18) in the first WLL fluid was measured 1 day post-exposure for the 80 $\mu\text{g}/\text{mouse}$ dose level for both NiO-NP and CeO₂-NP. Levels present were measured using commercially available ELISA kits (BioSource, Camarillo, CA) as previously described (Hamilton et al. 2009). To determine cathepsin B activity, in 96-well plates [using PBS as diluent], first WLL fluid (50 μl), 2 μg Z-LR-AMC (fluorogenic Peptide Substrate, R&D Systems, Minneapolis, MN) \pm 66 μM inhibitor (Z-Phe-Phe-FMK, MBL International, Woburn, MA) were combined in a total volume of 150 μl . The samples were incubated at 37°C for 1 hr before fluorescence was measured using a plate reader with 380 nm excitation and 460 nm emission. Cathepsin B specific activity was calculated as: relative fluorescence units (RFU) from cathepsin B activity (no inhibitor) minus with inhibitor.

Statistical analysis

Statistical Analysis was conducted using SigmaStat[®] Statistical Analysis Software. Comparisons among doses was performed for each particle-suspension media combination at all post-exposure times using an analysis of variance (ANOVA) with significance set at $p = 0.05$, with *post-hoc* tests for pair-wise comparison of dose groups. Analyses were conducted comparing pulmonary bioactivity of each CeO₂-NP and NiO-NP/suspension media combination to control at each post-exposure timepoint. Comparisons of bioactivity responses between poorly- and well-dispersed CeO₂-NP and NiO-NP/suspension media combination for each dose was also conducted for each post-exposure timepoint. Individual means were compared using a Tukey-pairwise multiple comparison procedure with an overall significance level of 0.05. Data are reported as mean \pm standard error (SE).

Results

Particle Characterization

DLS and zeta potential measurements were made on each media/NP combination (Tables 1 and 2). After 5 min of sonication, with both CeO₂-NP and NiO-NP suspensions, there were relatively large agglomerates in all four dispersion solutions. After 5 min of sonication, NiO-NP and CeO₂-NP suspended in DM had the smallest hydrodynamic diameter (489.9 and 302.6 nm, respectively) while the NiO-NP and CeO₂-NP suspended in Survanta[®] (5 min sonication) and pluronic (20 min sonication) had the largest agglomerates at 4460.1 and 694.2 nm, respectively (Table 1).

When comparing the hydrodynamic diameters of the NiO-NP and CeO₂-NP suspensions, there were no significant differences between the two metal oxide NP with regard to mean particle size in solution or zeta potential after either 5 or 20 min sonication (Tables 1 and 2). For example, after 5 min of sonication, the NiO-NP suspended in PBS had a mean diameter of 1312.5 nm while after 5 min of sonication the CeO₂-NP suspended in PBS had a mean diameter of 1726.2 nm. However, increasing sonication time from 5 to 20 min did significantly reduce the mean diameter of both CeO₂-NP and NiO-NP in all four dispersion solutions. The mean diameter of the CeO₂-NP suspended in DM after 5 min of sonication was 302 nm, but after increasing the sonication time to 20 min, the mean diameter of the CeO₂-NP significantly decreased to 89.3 nm (Table 1). Also, for both CeO₂-NP and NiO-NP suspensions, the particles dispersed in DM produced the smallest hydrodynamic diameter at the end of either sonication period (Figures 1A and 1B, Table 1). In comparison, CeO₂-NP and NiO-NP suspended in Survanta[®] produced particles with the largest hydrodynamic diameter after 5 min sonication, while after 20 min the particles suspended in pluronics had the largest diameter. BET surface area analysis of both NP in their dry state was measured. The BET specific area of NiO-NP was 113.0 m²/g while that of CeO₂-NP was 46.8 m²/g.

Role of pre-exposure dispersion status on lung inflammation and injury from CeO₂-NP

At 1 and 7 day post-exposure, there were no significant differences in PMN numbers (marker of inflammatory response) when comparing the various dispersed particle combinations for the CeO₂-NP+pluronic irrespective of dose (Figure 2). For CeO₂-NP dispersed in PBS, at 1 day post-exposure, a significant difference in PMN numbers between the poorly- and well-dispersed particle combinations was observed at both intermediate (40 µg/mouse) and high (80 µg/mouse) doses (Figure 2). At 7 day post-exposure, the well-dispersed CeO₂-NP/PBS combination caused a significant increase in PMN numbers at all doses compared to the poorly-dispersed CeO₂-NP/PBS combinations. Similar to the CeO₂-NP/pluronic combination, for CeO₂-NP dispersed in Survanta[®] at 1 day post-exposure, there were no significant differences in PMN numbers compared with the various dispersed particle/media combinations. However, at 7 day post-exposure, the well-dispersed CeO₂-NP +Survanta[®] caused a significant increase in PMN number when compared to the poorly-dispersed CeO₂-NP+Survanta[®] combinations.

For the CeO₂-NP dispersed in DM, no significant difference existed at 1 day post-exposure between the well-dispersed and poorly-dispersed particle/media combinations at any dose.

However, at 7 day post-exposure, the well-dispersed CeO₂-NP+DM produced a significant increase in PMN number at all doses when compared to the poorly-dispersed combinations. (NiO-NP PMN data shown in Figure 2 can be found in Sager et al. 2016).

LDH activity in lung lavage fluid was measured to assess cytotoxicity of CeO₂-NP/media combinations at 1 and 7 day post-exposure. At both timepoints, significant differences in LDH activity were seen when comparing the poorly- to well-dispersed particle combinations for CeO₂-NP+pluronics at the two highest doses (Figure 3, Panel A). In contrast, at 1 day post-exposure, no significant differences existed in LDH activity when comparing the poorly- and well-dispersed particle combinations for CeO₂-NP+PBS at any dose. At 7 day post-exposure, the highest dose of well-dispersed CeO₂-NP+PBS caused a significant increase in LDH activity when compared to poorly-dispersed CeO₂-NP+PBS. Well-dispersed CeO₂-NP+Survanta[®] caused a significant increase in LDH activity when compared to poorly-dispersed CeO₂-NP+Survanta[®] at both 1 and 7 day post-exposure, at all doses. In a similar manner, well-dispersed CeO₂-NP+DM produced a significant increase in LDH activity when compared to the poorly-dispersed particle/media combination at both 1 and 7 days post-exposure, at all doses. Taken together, the suspension studies showed that the well-dispersed particle suspensions were generally more cytotoxic when DM and Survanta[®] were dispersants, these provided the smallest agglomerates and highest bioactivity (NiO-NP LDH data shown in Figure 3 can be found in Sager et al. 2016).

NLRP3 inflammasome activation

To determine if either NiO-NP and/or CeO₂-NP/suspension combinations cause phago-lysosomal lysis and activation of the NLRP3 inflammasome, cathepsin B activities, as well as IL-18 and IL-1 β levels were measured (respectively) in the first WLL fluid collected from mice 1 day after exposure for each CeO₂-NP and NiO-NP/media combinations. Both CeO₂-NP and NiO-NP (Figure 4) produced a dose-dependent increase in cathepsin B activity, regardless of dispersion media type. In regards to differences based on dispersion, for both CeO₂-NP and NiO-NP, well-dispersed NP/suspension combinations produced significantly more cathepsin B release compared to poorly-dispersed NP/suspension combinations. When comparing the NiO-NP/combinations to the CeO₂-NP/combinations, NiO-NP/suspension combinations resulted in an \approx 20% greater increase in levels of cathepsin B activity than CeO₂-NP/suspension combinations.

IL-18 levels for animals receiving NiO-NP dispersed in pluronics or PBS were not significantly different than control levels of IL-18 at any dose (Figure 5). However, the well-dispersed NiO-NP in Survanta[®] and DM did significantly increase IL-18 at all doses compared to control. Furthermore, the well-dispersed NiO-NP Survanta[®] and DM media combinations produced a significant increase in IL-18 at all doses compared to the corresponding poorly-dispersed NiO-NP Survanta[®] and DM media combinations. The two highest doses of all the CeO₂-NP/media combinations produced a significant increase in IL-18 in the WLL compared to control, as well as compared to their corresponding poorly-dispersed counterparts.

IL-1 β levels of NiO-NP dispersed in pluronics or PBS showed no trends in regard to dose or dispersion (Figure 6). However, the highest doses of the well-dispersed NiO-NP/Survanta[®]

and DM combinations produced a significant increase in IL-1 β compared to control (Figure 6). For the CeO₂-NP pluronics combination, the two highest doses produced a significant increase in IL-1 β compared to control. For the CeO₂-NP PBS and Survanta[®] combinations, all doses of the well-dispersed particle/media combinations produced a significant increase in IL-1 β compared to control, respectively. The highest dose of the CeO₂-NP/DM combination produced a significant increase in IL-1 β compared to control.

Taken together, the studies demonstrated that the well-dispersed particle suspensions facilitated activation of the NLRP3 inflammasome via pro-inflammatory cytokine production and cathepsin B release with DM and Survanta[®] as dispersants to a greater extent than the poorly dispersed particle suspensions in the same dispersing agents.

Electron Spin Resonance Studies

ESR studies were conducted to assess whether ROS production mediated the pulmonary bioactivity of CeO₂-NP and NiO-NP. In order to better interpret where within the cells the particles were localizing and stimulating production of ROS, ESR was measured in a two-system set-up. First, radical generation facilitated by each nanoparticle was measured in artificial lysosome fluid (ALF), a fluid that mimics the lysosome acidic environment (ALF pH~4.5), or dispersion media (DM pH~7.4) that mimics the pH in a cell cytosol. Figure 7 shows results of measurements of radicals after the particles were exposed to a superoxide-generating system in ALF. CeO₂-NP significantly decreased radical production, indicating a scavenging of superoxide radicals generated from xanthine/xanthine oxidase reaction. In contrast, NiO-NP had no significant effect in the ALF system on measured radicals compared to controls with no particles. When the reaction took place in DM (an experimental set-up used to mimic particle environment in a cell cytosol), NiO-NP reduced radical levels compared to the controls, while CeO₂-NP had no apparent effect.

These findings indicate NiO-NP would likely be a better scavenger of radicals than CeO₂-NP in a cell cytosol, whereas the opposite is the case in an acidic environment (resembling internal environment of lysosome). Specifically, CeO₂-NP were shown to scavenge radicals in the ALF (pH~ 4.5) experimental environment but had no scavenging behavior in a physiological pH (7.4) experimental environment. Therefore, from the ESR analysis, it can be concluded the difference in scavenging abilities of NiO-NP and CeO₂-NP appears pH-related. However, in neither experimental environment did either metal oxide increase ROS production.

Discussion

The current study was performed to evaluate how specific particle parameters, i.e. pre-exposure dispersion status and particle surface area, of two highly utilized metal oxide NP (NiO and CeO₂) influence inflammasome activation during ENM-induced toxicity. First, this study assessed whether pre-exposure dispersion differences (like mean hydrodynamic diameter in various medias) of each utilized NP could be facilitating differences in pulmonary bioactivity between the two particles. As studies from our laboratory have previously reported, dispersion of NP can be improved using various suspension strategies. For example, *in vivo* and *in vitro* studies have used a variety of dispersants, including media

that mimic the alveolar fluid lining of the lung (Hamilton et al. 2009; Sager et al. 2014), 1% Tween 80 in PBS (Muller et al. 2005; Warheit et al. 2004) and cell culture media (Shvedova et al. 2003). For all biological applications of NP, it is important to understand the interactions a NP has with the surrounding biological environment to allow better prediction of their biological impact. When exposed to biological fluids, proteins and biomolecules in the medium tend to associate with the NP surface. In many cases the dispersion media used to make the particle suspension may alter the surface reactivity of the NP, in turn, modifying its toxicity. Therefore, either delivering agglomerated NP or using a dispersion media that coats the particle could lead to variability in assessment of toxicity of a specific NP.

In the current study, NiO was chosen since we and others reported that NiO NP stimulate pulmonary inflammation and injury (Asati et al. 2010; Horie et al. 2011; Sager et al. 2016). CeO₂ was chosen for comparison due to the evidence that it can display either a beneficial (anti-oxidant) or toxic (oxidant) effect (Asati et al. 2010) under differing experimental situations. The current study demonstrated that pharyngeal aspiration of mice with CeO₂-NP produced inflammation (an increase in PMN), as well as promoted cell injury (enhanced LDH activity in first WLL fluid) *in vivo*. Previously, our laboratory has shown that pharyngeal aspiration of mice with NiO-NP resulted in very similar trends in inflammation and cell injury over the course of 7 day post-exposure (Sager et al. 2016). General trends that were common between the CeO₂-NP and NiO-NP exposures were: 1) a greater response 7 day post-exposure compared to 1 day post- aspiration; 2) dose dependence from 20–80 µg/mouse; and, 3) a relationship between degree of dispersion and pulmonary response.

The various physicochemical parameters of ENM, such as size, shape, structure, and elemental constituents, make the investigation of their toxic effects complex and challenging (Pojlak-Blazi et al. 2010). Some of the paradigms for ENM-mediated toxicity include oxidative stress, inflammation, genetic damage, and the inhibition of cell division and cell death (Stone et al. 2007; Ju-Nam and Lead, 2008; Li et al. 2008; Johnston, et al. 2010). Many studies suggest that ROS generation and in turn, consequent oxidative stress and inflammasome activation are frequently associated with ENM toxicity (Nel et al. 2006; Shevdova et al. 2012). The physico-chemical characterization of ENM including particle size, surface charge, and chemical composition is a key indicator for the resulting ROS response and injury, since many intrinsic properties of ENM have been proposed to be associated with ROS production (Nel et al. 2006). However, it may be inaccurate to assume ROS generation is a prerequisite for all inflammasome activation and ENM-induced toxicity. In fact, some studies have reported the direct toxicity of ENM without ROS generation (Wang et al. 2010). Nevertheless, ROS generation facilitating inflammasome activation may be a major event during ENM-induced injury that needs to be thoroughly characterized in order to predict ENM-induced toxicity.

In contrast to the general assumption of ENM-induced ROS generation, a unique NP, CeO₂, has been suggested as having anti-oxidant properties (Tarnuzzer et al. 2006; Perez et al. 2008; Asati et al. 2010). In fact, the chemistry of engineered CeO₂ NP supports its role of a biological free radical scavenger or anti-oxidant, since CeO₂ nanoparticles cycle between Ce⁺³ and Ce⁺⁴ valence states. This means they possess oxygen vacancies that allow the NP to act as a regenerative catalyst (Heckert et al. 2008). CeO₂-NP have been identified as one

of the most economically valuable manufactured NP in current production (Wang et al. 2008). CeO₂ demonstrates high oxygen storage capabilities, high oxygen ionic conductivity, as well as strong absorption of UV radiation (Lui et al. 2013). Thus, CeO₂-NP are widely utilized in a variety of applications ranging from glass and ceramic polishing agents (Eom and Choi, 2009) to solar panels and fuel cells (Corma et al. 2004). Along with many industrial applications, a variety of biomedical applications utilizing CeO₂-NP have also been explored. For example, CeO₂-NP are currently being utilized to protect against ultra-violet radiation induced damage.

Studies from our laboratory show that both NiO-NP (Sager et al. 2016) and CeO₂-NP promote divergent pulmonary inflammatory responses. Characterization of pre-exposure dispersion status was explored as a possible variable contributing to the differences in bioactivity. The DLS experiments showed that increasing the sonication time from 5 min to 20 min significantly decreased the hydrodynamic diameter of each particle suspension. For example, after 5 min sonication, CeO₂-NP suspended in DM had a hydrodynamic diameter of 302.6 nm. However, upon increasing the sonication time to 20 min, the hydrodynamic diameter of the CeO₂-NP suspended in DM significantly decreased to 89.3 nm. There were no significant differences with regard to average hydrodynamic diameter size between NiO-NP and CeO₂-NP suspended in the same media after 5 or 20 min sonication, representing poorly dispersed or well dispersed suspensions respectively. For example, after 20 min sonication, the average diameter of NiO-NP suspended in PBS was 486.8 nm while that of CeO₂-NP in PBS was 568.6 nm. Therefore, pre-exposure dispersion status was subsequently ruled out as a probable variable to explain differences in bioactivity between the two particles.

Another possible variable affecting ENM bioactivity is activation of the NLRP3 inflammasome following phagolysosomal membrane permeability and cathepsin B release. Current evidence suggests that bioactive nanoparticles could potentially increase phagolysosomal membrane permeability, causing release of cathepsin B and activation of the NLRP3 inflammasome with subsequent release of IL-1 β and IL-18 from alveolar macrophages (Beamer et al. 2012). It has been shown previously that the NLRP3 inflammasome is activated *in vivo* after pulmonary exposure to MWCNT (Sager et al. 2014). In addition to the phagolysosomal release of cathepsin B, other possible NLRP3 inflammasome activation pathways have been explored. In addition to engaging the phagocytic pathway to activate the NLRP3 inflammasome, a second model of NLRP3 inflammasome activation suggests increased production of ROS activates the NLRP3 inflammasome (Halle et al. 2008; Jin and Flavell, 2010).

With regard to the first model of inflammasome activation, the results showed that both NiO-NP and CeO₂-NP facilitated a significant increase in cathepsin B release. However, for cathepsin B release, there was no significant difference between the effects of NiO-NP and CeO₂-NP. Both NiO-NP and CeO₂-NP (well-dispersed, 80 μ g/mouse, 1 day post-exposure) produced a significant increase not only in cathepsin B, but also in levels of IL-1 β and IL-18. Cathepsin B levels were not significantly different between NiO-NP- and CeO₂-NP-exposed mice. However, mice exposed to 80 μ g NiO-NP did have a greater increase in inflammatory IL-1 β and IL-18. Thus, due to the similar trend in cathepsin B levels for the

NiO-NP- and CeO₂-NP-exposed mice, it was concluded that both ENM facilitated NLRP3 inflammasome activation via phagolysosome disruption. However, differences in responses of IL-1 β and IL-18 between NiO-NP- and CeO₂-NP-exposed mice may not be explained solely by cathepsin B release.

ESR studies were conducted to identify whether ROS production played a role in facilitating the difference in bioactivity between the NiO-NP and CeO₂-NP. Previous studies identified CeO₂ as a unique nanomaterial because it can, in certain experimental situations, exhibit anti-inflammatory properties. More specifically, CeO₂ has been reported to scavenge ROS/possess superoxide-dismutase-like activity (Korsvik et al. 2007; Perez et al. 2008). If this was in fact, the case, CeO₂ acting as an anti-oxidant could help explain the difference in the bioactivities of the two types of NP here.

Previous studies [Asati et al. 2010] reported that nanoceria displayed optimal anti-oxidant properties at physiological pH, but behaves as an oxidase at acidic pH. Asati et al. also reasoned that CeO₂-NP cytotoxicity could depend on subcellular localization. Once in a cell, NP toxicity could depend on whether the NP are localized in particular cellular organelles (such as lysosomes which are acidic) or distributed in the cytoplasm (which is at neutral pH). However, the outcome of the current ESR studies showed that in an acidic environment (ALF, pH~ 4.5) mimicking the lysosome internal environment, CeO₂-NP acted as a scavenger, significantly reducing free radicals. At a physiological pH (DM, pH ~ 7.4) to mimic cell cytosol, CeO₂-NP did not scavenge radicals. In contrast, NiO-NP at a physiological pH (in DM) did significantly scavenge free radicals; in an acidic environment (ALF) NiO-NP did not reduce radicals. This outcome supports the conclusions of previously-published studies that concluded there was a role for pH as a facilitator of the anti-oxidant behavior of CeO₂. Furthermore, these findings also indicate that ENM, once co-localized inside a cell, do not require increased ROS production to activate the NLRP3 inflammasome.

Conclusions

Taken together, the current study showed that pre-exposure dispersion status was a factor that contributed to the post-exposure pulmonary bioactivity. This study showed that the smaller the hydrodynamic diameter of a particle suspension, the greater the pulmonary bioactivity of the particle suspension. However, pre-exposure dispersion differences between NiO-NP suspensions and CeO₂-NP suspensions used in this study cannot contribute to helping explain the difference between pulmonary bioactivities of NiO-NP and CeO₂-NP. These differences in bioactivity are likely due in part to NiO-NP facilitating production of IL-1 β and IL-18. Further, in this study, both oxides acted as free radical scavengers, depending on the experimental environmental pH. CeO₂-NP acted as free radical scavenger in an environment mimicking a lysosome while NiO-NP acted as scavenger in a physiological pH (environment mimicking cytosol). Another possible factor contributing to the difference in bioactivity of the CeO₂-NP and NiO-NP may be the vast difference in their surface area; BET specific area of NiO-NP was 113.0 m²/g while that of CeO₂-NP was 46.8 m²/g. Similar results have been noted in comparing pulmonary responses to ultrafine and

fine titanium dioxide (Sager et al. 2008). Therefore, specific surface area may help explain the differences in bioactivity of ENM.

Acknowledgments

The authors would like to thank Diane Schwegler-Berry for her assistance on obtaining the TEM and SEM images presented in the MS. Mention of brand name does not constitute product endorsement. The findings and conclusions in this report are those of the authors and do not necessarily represent the views of the National Institute for Occupational Safety and Health.

Funding

This work was supported by NIH grant F32 ES021341.

Abbreviations

ALF	Artificial lysosomal fluid
AM	Alveolar macrophage
ANOVA	Analysis of variance
BAL	Bronchoalveolar lavage
BET	Brunauer-Emmett-Teller
CeO₂	Cerium oxide
CeO₂-NP	Cerium oxide nanoparticles
CAR	Cilia-associated-respiratory
DLS	Dynamic light scattering
DM	Dispersion media
DMPO	5,5-dimethyl-1-pyrroline-oxide
ENM	Engineered nano-materials
ESR	Electron spin resonance
FESEM	Field emission scanning electron microscopy
IL	Interleukin
IP	Intraperitoneal
K₃CrO₈	potassium tetra-peroxochromate
LDH	Lactate dehydrogenase
µm	Micrometer
µg	Microgram
mg	Milligram

ml	Milliliter
mm	Millimeter
NiO	Nickel oxide
NiO-NP	Nickel oxide nanoparticles
NP	nanoparticle
PBS	Phosphate-buffered saline
PMN	Polymorphonuclear leukocyte
PD	poorly-dispersed
RFU	Relative fluorescence units
TEM	Transmission electron microscopy
WD	Well-dispersed
WLL	Whole lung lavage

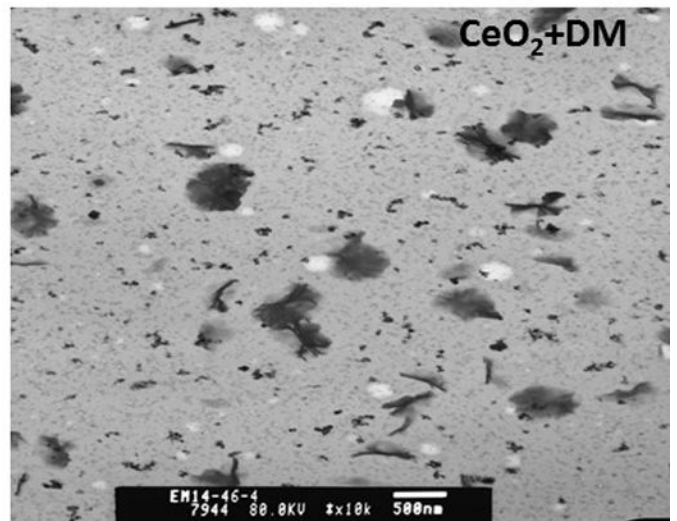
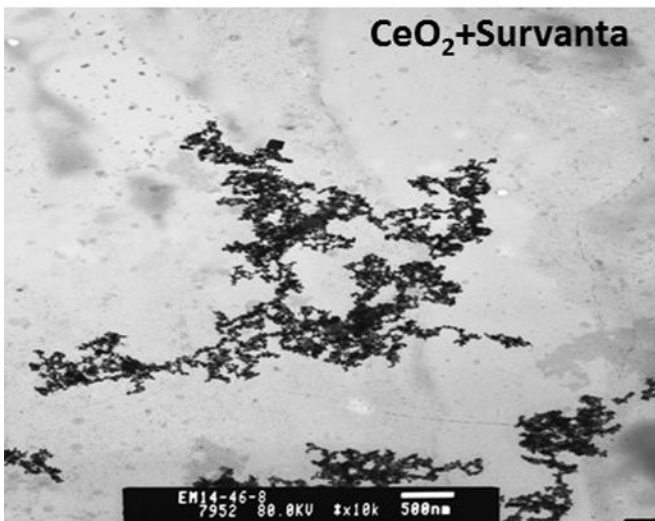
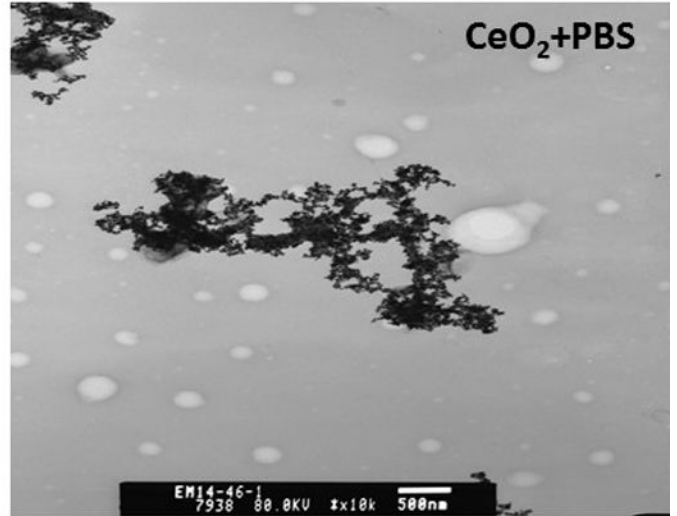
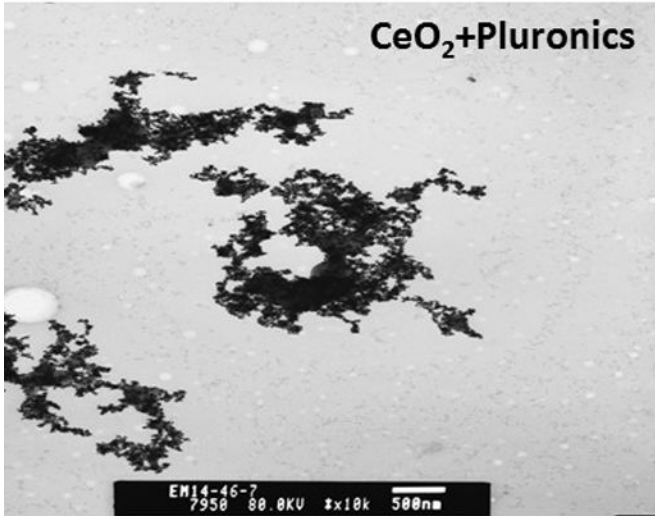
References

- Asati A, Santra S, Kaitanis C, Perez M. Surface-charge-dependent cell localization and cytotoxicity of cerium oxide nanoparticles. *ACS Nano*. 2010; 4:5321–5331. [PubMed: 20690607]
- Auffan M, Bottero J, Chaneac C, Rose J. Inorganic manufactured nanoparticles: How their physico-chemical properties influence their biological effects in aqueous environments. *Nanomedicine*. 2010; 5:999–1007. [PubMed: 20735233]
- Beamer C, Girtsman T, Seaver B, Finsaas K, Migliaccio C, Perry V. IL-33 mediates multi-walled carbon nanotube (MWCNT)-induced airway hyper-reactivity via the mobilization of innate helper cells in the lung. *Nanotoxicology*. 2012; 7:1070–1081. [PubMed: 22686327]
- Brunauer S, Emmett PH, Teller E. Adsorption of gases in multi-molecular layers. *JACS*. 1938; 60:309–319.
- Chithrani B, Ghazani A, Chan W. Determining the size and shape dependence of gold nanoparticle uptake into mammalian cells. *Nano Lett*. 2006; 6:662–668. [PubMed: 16608261]
- Corma A, Atienzar P, Garcia H, Chane-ching J. Hierarchially-meso-structured doped CeO₂ with potential for solar-cell use. *Nat Mater*. 2004; 3:394–397. [PubMed: 15146175]
- Donaldson K, Brown D, Clouter A, Duffin R, MacNee W, Renwick L, Tran L, Stone V. The pulmonary toxicology of ultrafine particles. *J Aerosol Med*. 2002; 15:213–220. [PubMed: 12184871]
- Eom H, Choi J. Oxidative stress of CeO₂ nanoparticles via p38-Nfr-2 signaling pathway in human bronchial epithelial cell, Beas-2B. *Toxicol Lett*. 2009; 187:77–83. [PubMed: 19429248]
- Gillespie P, Kang G, Elder A, Gelein R, Chen L, Moreira A. Pulmonary response after exposure to inhaled nickel hydroxide nanoparticles: Short and long-term studies in mice. *Nanotoxicology*. 2010; 4:106–109. [PubMed: 20730025]
- Halle A, Hornung V, Petzold G, Stewart C, Monks B, Reinheckel T. The NALP3 inflam-masome is involved in the innate immune response to amyloid- β . *Nat Immunol*. 2008; 9:857–865. [PubMed: 18604209]
- Hamilton R, Wu N, Porter D, Buford M, Wolfarth M, Holian A. Particle length-dependent titanium dioxide nanomaterials' toxicity and bioactivity. *Particle Fiber Toxicol*. 2009; 6:35–41.
- Heckert E, Karakoti A, Seal S, Self W. The role of cerium redox state in the SOD mimetic activity of nanocerium. *Biomaterials*. 2008; 29:2705–2709. [PubMed: 18395249]

- Horie M, Fukui H, Nishio K, Endoh S, Kato H, Fujita K. Evaluation of acute oxidative stress induced by NiO₂ nanoparticles *in vivo* and *in vitro*. *Metallomics*. 2011; 11:1244–1252.
- Jin C, Flavell R. The missing link: How the inflammasome senses oxidative stress. *Immunol Cell Biol*. 2010; 88:510–512. [PubMed: 20458338]
- Johnston H, Hutchison G, Christensen F, Peters S, Hankin S, Stone V. A review of the *in vivo* and *in vitro* toxicity of silver and gold particulates: Particle attributes and biological mechanisms responsible for the observed toxicity. *Crit Rev Toxicol*. 2010; 40:328–346. [PubMed: 20128631]
- Ju-Nam Y, Lead J. Manufactured nanoparticles: Overview of their chemistry, interactions and potential environmental implications. *Sci Total Environ*. 2008; 400:396–414. [PubMed: 18715626]
- Keller A, Wang H, Zhou D. Stability and aggregation of metal oxide nanoparticles in natural aqueous matrices. *Environ Sci Technol*. 2010; 44:1962–1967. [PubMed: 20151631]
- Korsvik C, Patil S, Seal S, Self W. Vacancy engineered ceria oxide nanoparticles catalyze superoxide dismutase activity. *Chem Commun*. 2007; 35:1056–1058.
- Lewinski N, Colvin V, Drezek R. Cytotoxicity of nanoparticles. *Small*. 2008; 4:26–49. [PubMed: 18165959]
- Li JJ, Muralikrishnan S, Ng CT, Yung LY, Bay HB. Nanoparticle-induced pulmonary toxicity. *Experimental Biology and Medicine*. 2010; 235(9):1025–1033. [PubMed: 20719818]
- Li N, Xia T, Nel A. The role of oxidative stress in ambient particulate matter-induced lung diseases and its implications in the toxicity of engineered nanoparticles. *Free Rad Biol Med*. 2008; 44:1689–1699. [PubMed: 18313407]
- Lui T, Hon M, Teoh L. Structure and optical properties of CeO₂ nanoparticles synthesized by precipitation. *J Elect Mater*. 2013; 42:2536–2543.
- Manke A, Wang L, Rojanasakul Y. Mechanisms of nanoparticle-induced oxidative stress and toxicity. *Bio-Med Res Intl*. 2013; 201:1–15.
- Marques M, Loebenberg R, Almukainzi M. Simulated biological fluids with possible application in dissolution testing. *Dissol Technol*. 2011:15–28.
- Monteiller C, Tran L, MacNee W, Faux S, Jones A, Miller B, Donaldson K. The pro-inflammatory effects of low-toxicity low-solubility particles, nanoparticles and fine particles, on epithelial cells *in vitro*: Role of surface area. *Occup Environ Med*. 2007; 64:609–615. [PubMed: 17409182]
- Murphy C, Gole A, Stone J. Gold nanoparticles in biology: Beyond toxicity to cellular imaging. *Acc Chem Res*. 2008; 41:1721–1730. [PubMed: 18712884]
- Nel A, Xia T, Madler L, Li N. Toxic potential of materials at the nanolevel. *Science*. 2006; 311:622–627. [PubMed: 16456071]
- Perez JM, Asati A, Nath S, Kaittanis C. Synthesis of biocompatible dextran-coated nanoceria with pH-dependent anti-oxidant properties. *Small*. 2005; 4:552–556.
- Pojlak-Blazi, M., Jaganjac, M., Zarkovic, N. *Handbook of Nanophysics: Nanomedicine and Nanorobotics*. New York: CRC Press; 2010. Cell oxidative stress: Risk of metal nanoparticles; p. 17-22.
- Porter D, Barger M, Robinson V, Leonard S, Landsittel D, Castranova V. Comparison of low doses of aged and freshly fractures silica on pulmonary inflammation and damage in the rat. *Toxicology*. 2002; 175:63–71. [PubMed: 12049836]
- Powers K, Palazuelos M, Moudgil B, Roberts S. Characterization of the size, shape, and state of dispersion of nanoparticles for toxicological studies. *Nanotoxicology*. 2007; 1:42–51.
- Rao G, Tinkle S, Weissman D, Antonini J, Kashon M, Salmen R. Efficacy of a technique for exposing the mouse lung to particles aspirated from the pharynx. *J Toxicol Environ Health*. 2003; 66:1441–1452.
- Sager T, Porter D, Robinson V, Lindsley W, Schwegler-Berry D, Castranova V. Improved method to disperse nanoparticles for *in vitro* and *in vivo* investigation of toxicity. *Nanotoxicology*. 2007; 1:118–129.
- Sager T, Kommineni C, Castranova V. Pulmonary response to intratracheal instillation of ultrafine vs. fine titanium dioxide: Role of surface area. *Particle Fiber Toxicol*. 2008; 5:17.

- Sager T, Castranova V. Surface area of particle administered versus mass of particle administered in determining the pulmonary toxicity of ultrafine and fine carbon black: a sub-chronic in vivo exposure. *Particle Fiber Toxicol.* 2009; 6:1.
- Sager T, Wolfarth M, Andrews M, Hubbs A, Porter D, Wu N. Analysis of effect of multi-walled carbon nanotube surface modification on bioactivity and inflammasome activation. *Nanotoxicology.* 2014; 8:317–327. [PubMed: 23432020]
- Sager T, Wolfarth M, Keane M, Porter D, Castranova V, Holian A. Effects of nickel-oxide nanoparticle pre-exposure dispersion status on bioactivity in the mouse lung. *Nanotoxicology.* 2016; 10:151–161.
- Shvedova A, Pietroiusti P, Fadeel B, Kagan V. Mechanisms of carbon nanotube-induced toxicity: Focus on oxidative stress. *Toxicol Appl Pharmacol.* 2012; 261:121–133. [PubMed: 22513272]
- Stone V, Johnston H, Clift J. Air pollution, ultrafine and nanoparticle toxicology: Cellular and molecular interactions. *Trans Nanobiosci.* 2007; 6:331–340.
- Tarnuzzer R, Colon J, Patil S, Seal S. Vacancy engineered ceria nanostructures for protection from radiation-induced cellular damage. *Nano Lett.* 2005; 5:2573–2577. [PubMed: 16351218]
- Wang L, Mercer R, Rojanasakul Y. Direct fibrogenic effects of dispersed single-wall carbon nanotubes on human lung fibroblasts. *J Toxicol Environ Health.* 2010; 73:410–422.
- Wang R, Crozier P, Sharma R, Adams J. Measuring the redox activity of individual catalytic nanoparticles in cerium-based oxides. *Nano Lett.* 2008; 8:962–967. [PubMed: 18251517]
- Wang S, Lu W, Tovmachenko O, Rai U, Yu H, Ray P. Challenge in understanding size and shape dependent toxicity of gold nanomaterials in human skin keratinocytes. *Chem Phys Lett.* 2008; 463:145–149. [PubMed: 24068836]
- Zeidler P, Hubbs A, Battelli L, Castranova V. Role of inducible nitric oxide in silica-induced pulmonary inflammation and fibrosis. *J Toxicol Environ Health.* 2004; 67:1021–1026.

A



Author Manuscript

Author Manuscript

Author Manuscript

Author Manuscript

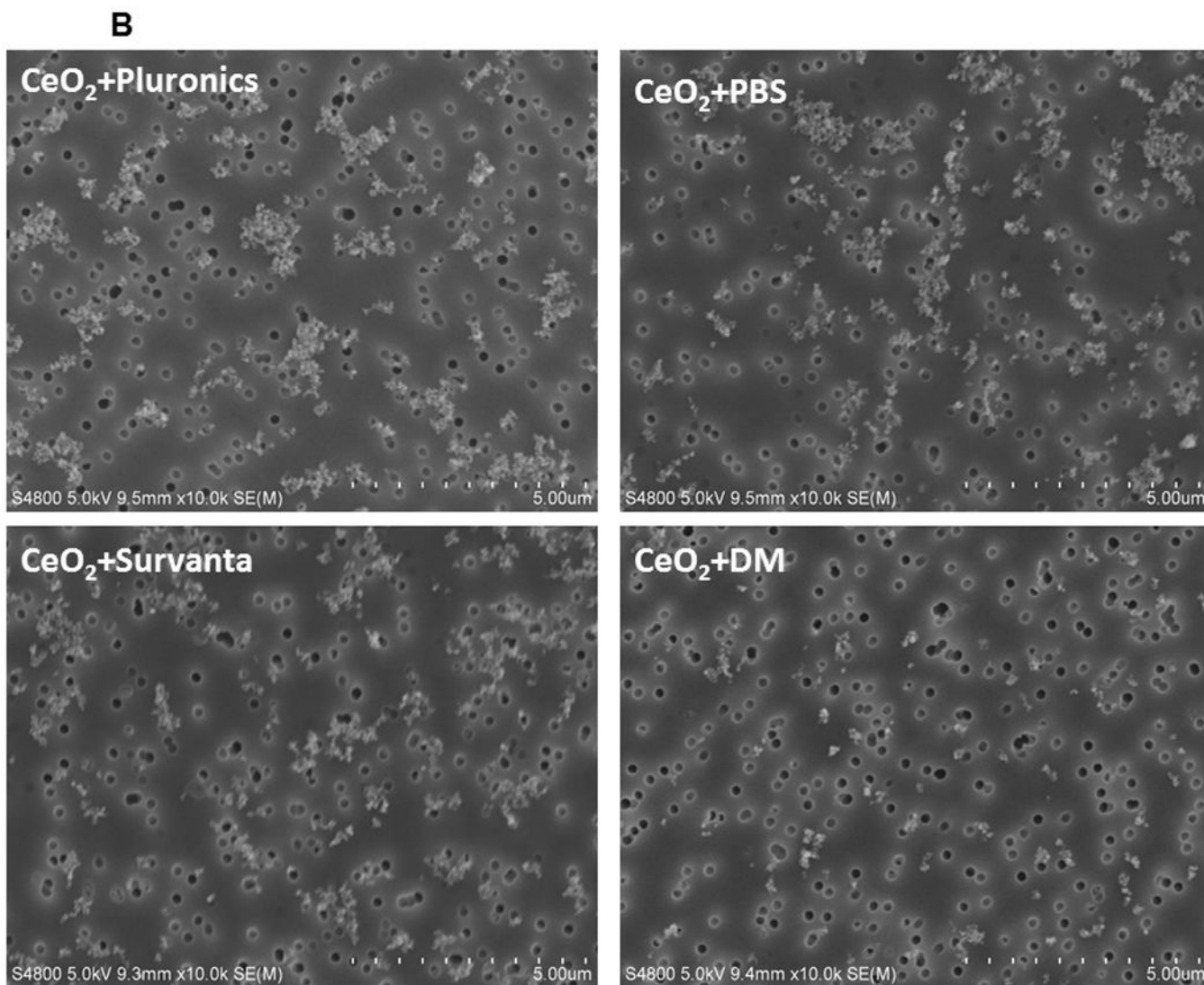


Figure 1.

Panel A. Transmission electron microscopy (TEM) micrographs of CeO₂-NP in pluronic (after 20 min sonication, well-dispersed, Panel A), PBS (after 20 min of sonication, well-dispersed, Panel B), Survanta[®] (after 20 min sonication, Well-dispersed, Panel C), and DM (after 20 min sonication, Well-dispersed, Panel D). Samples for TEM analyses were obtained from the same samples used for dynamic light scattering analyses (data presented in Table 1). **Panel B.** Field emission scanning electron microscopic (FESEM) micrographs of CeO₂-NP in pluronic (after 20 min sonication, well-dispersed, Panel A), PBS (after 20 min sonication, well-dispersed, Panel B), Survanta[®] (after 20 min sonication, well-dispersed, Panel C), and DM (after 20 min of sonication, well-dispersed, Panel D). Samples for FESEM analyses were obtained from the same samples used for dynamic light scattering analyses.

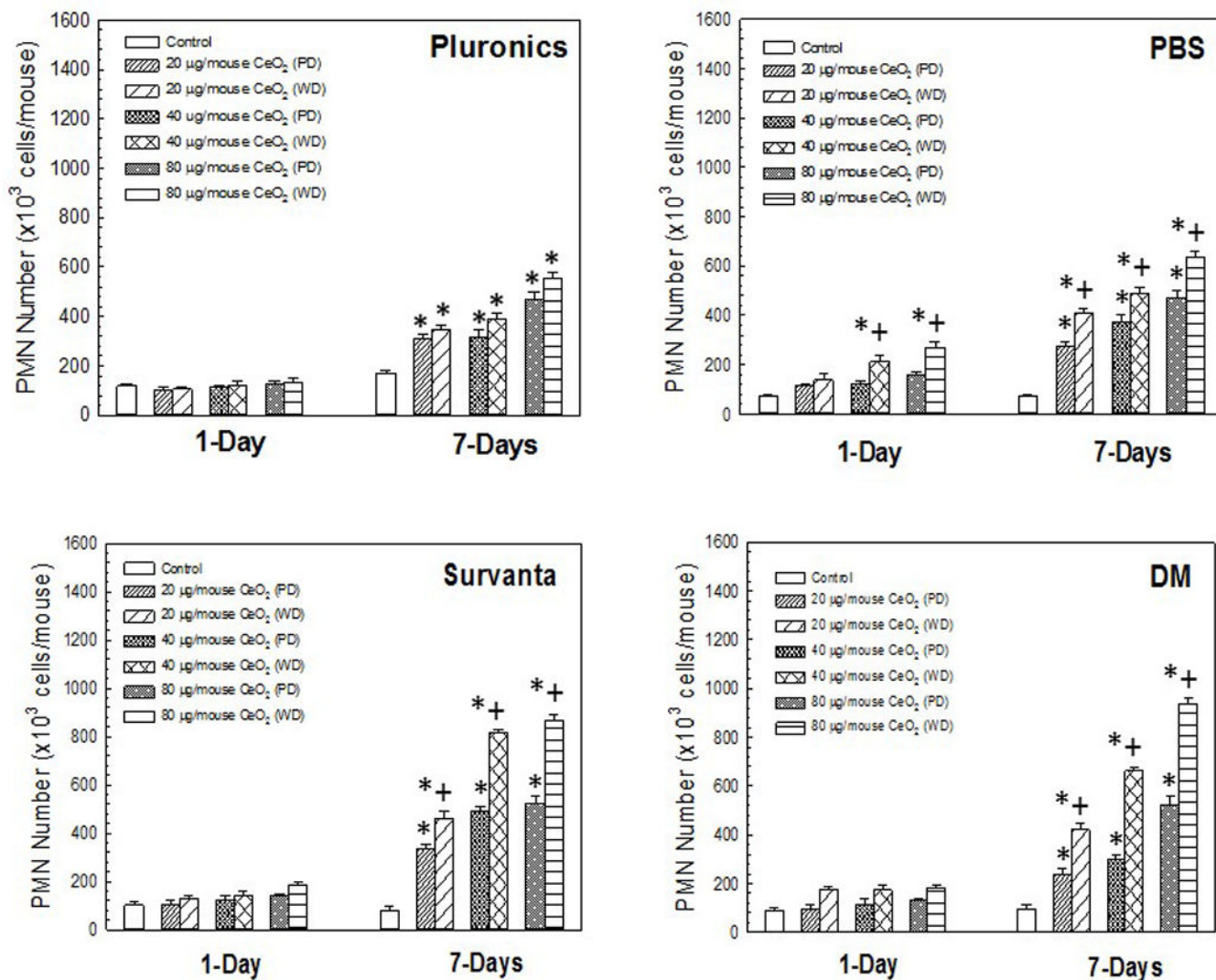


Figure 2.

PMN number induced by pharyngeal aspiration exposure to 0, 20, 40, or 80 µg/mouse of either poorly-dispersed (PD) or well-dispersed (WD) CeO₂-NP dispersed in differing dispersion medias (Panel A, pluronics, Panel B, PBS, Panel C, Survanta[®], and Panel D, DM) at 1 and 7 days post-exposure. Values are given as means ± SE (n=8). *Significant difference between treatment and control groups at 1 and 7 day post-exposure (p < 0.05). +Significant difference between well-dispersed (20 min sonication) and poorly-dispersed (5 min sonication) CeO₂-NP solutions at same post-exposure timepoint (p < 0.05). (NiO-NP PMN data shown in figure is from Sager et al. [2016]).

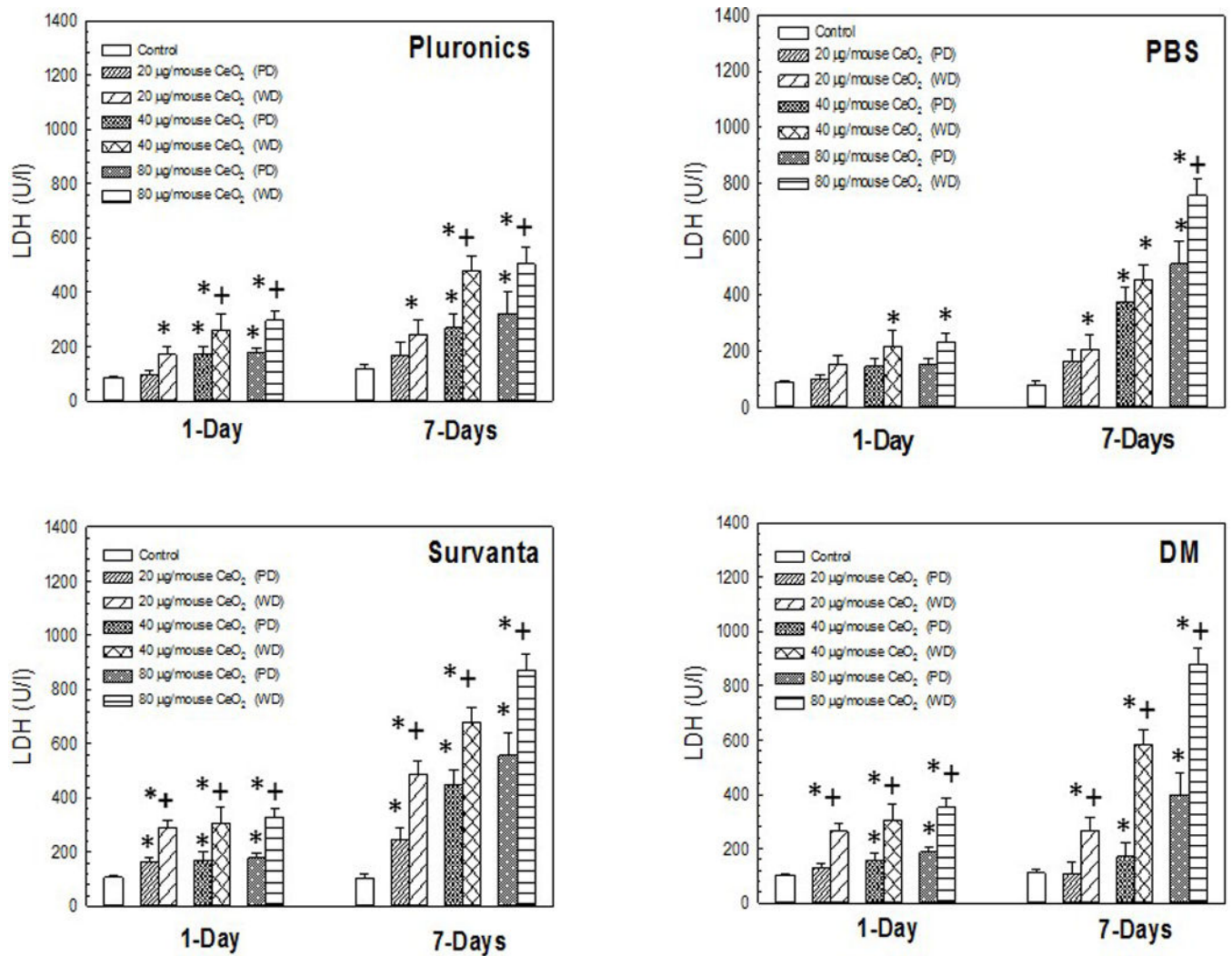


Figure 3.

LDH activity induced by pharyngeal aspiration exposure to 0, 20, 40, or 80 µg/mouse of either poorly-dispersed (PD) or well-dispersed (WD) CeO₂-NP dispersed in differing dispersion media (Panel A, Plurionics, Panel B, PBS, Panel C, Survanta[®], and Panel D, DM) at 1 and 7 day post-exposure. Values are given as means ± SE (n=8). *Significant difference between treatment group and control group 1 and 7 day post-exposure ($p < 0.05$). +Significant difference between well-dispersed (20 min sonication) and poorly-dispersed (5 min sonication) CeO₂-NP solutions at the same post-exposure time point ($p < 0.05$). (NiO-NP LDH data shown in figure from Sager et al. [2016]).

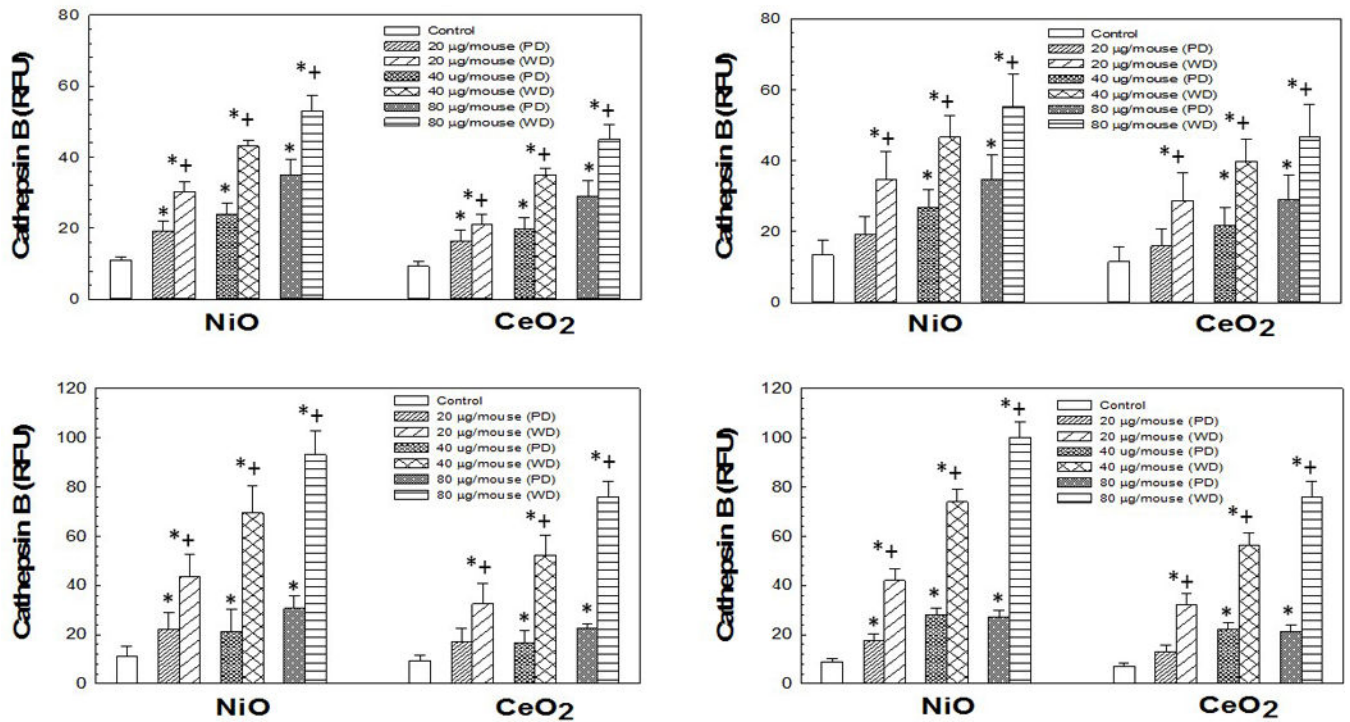


Figure 4.

Cathepsin B activities induced by pharyngeal aspiration exposure to 0, 20, 40, or 80 µg/mouse of either poorly-dispersed (PD) or well-dispersed (WD) NiO- and CeO₂-NP dispersed in differing dispersion medias (Panel A: pluronics, Panel B: PBS, Panel C: Survanta[®], and Panel D: DM) at 1 day post-exposure. Values are given as means ± SE (n=8). *Significant difference of treatment group from control at 1 day post-exposure ($p < 0.05$). +Significant difference between the poorly-dispersed (5 min sonication) and well-dispersed (20 min sonication) NiO- and CeO₂-NP solutions at same post-exposure timepoint ($p < 0.05$). Cathepsin B activities determined as described in Methods.

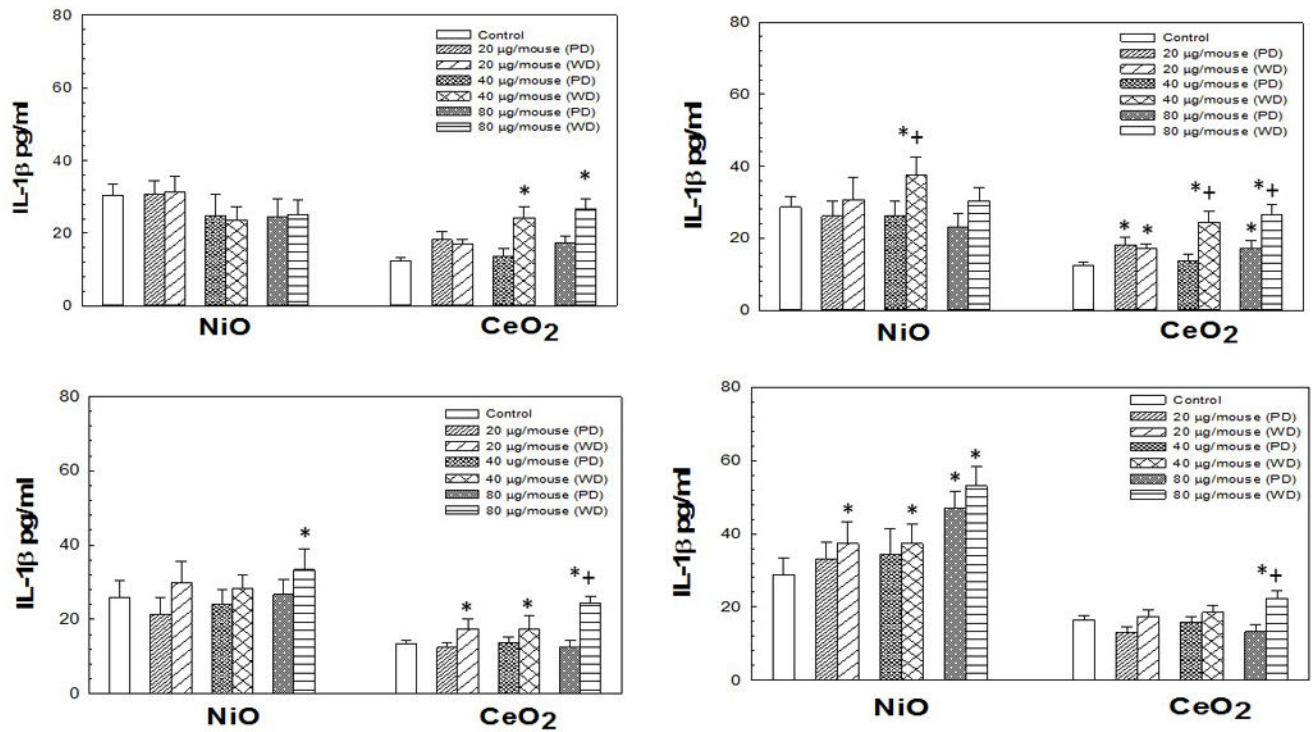


Figure 5.

IL-18 levels induced by pharyngeal aspiration exposure to 0, 20, 40, or 80 μ g/mouse of either poorly-dispersed (PD) or well-dispersed (WD) NiO- and CeO₂-NP dispersed in differing dispersion medias (Panel A: pluronic, Panel B: PBS, Panel C: Survanta[®], and Panel D: DM) at 1 day post-exposure. Values are given as means \pm SE (n=8). *Significant difference of treatment group from control at 1 day post-exposure ($p < 0.05$). +Significant difference between the poorly-dispersed (5 min sonication) and well-dispersed (20 min sonication) NiO- and CeO₂-NP solutions at same post-exposure timepoint ($p < 0.05$). IL-18 concentrations were determined as described in Methods.

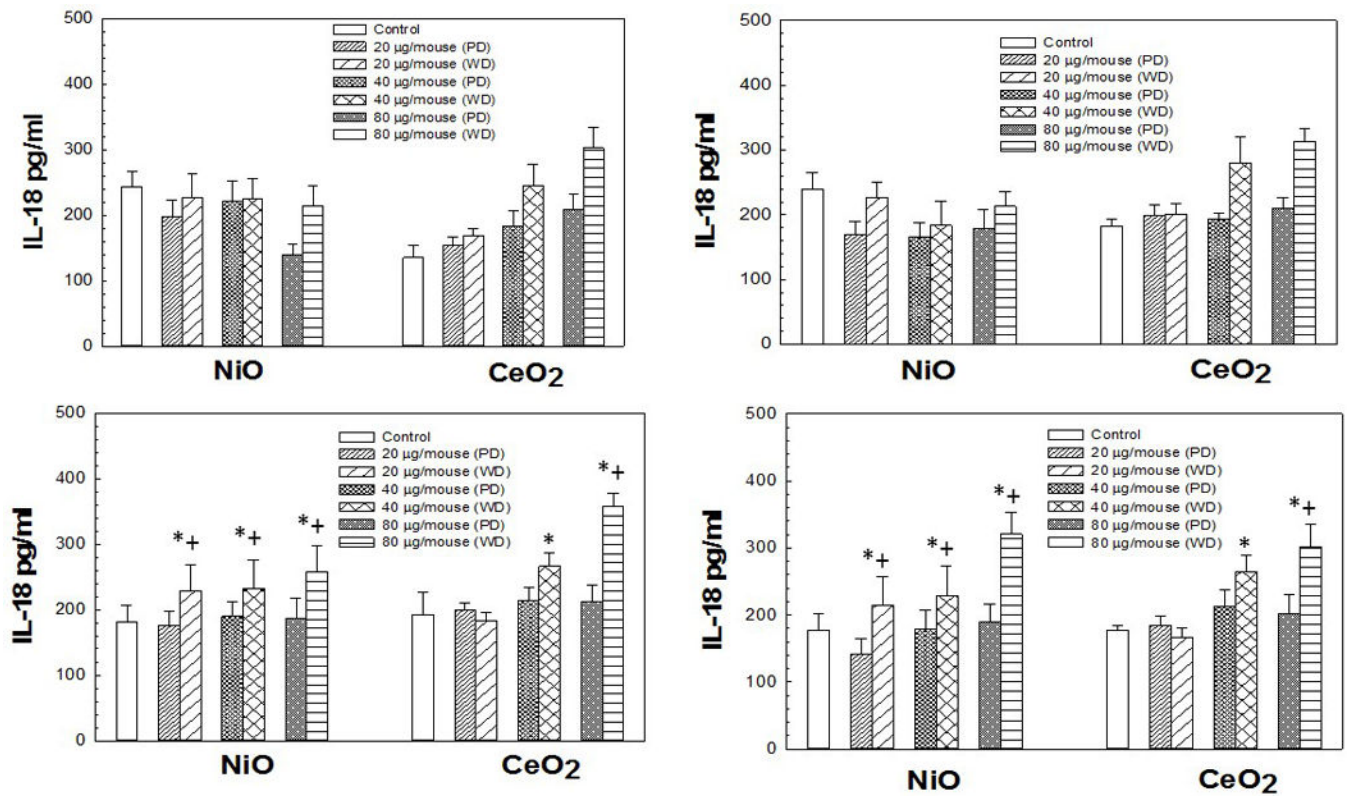


Figure 6.

IL-1 β levels induced by pharyngeal aspiration exposure to 0, 20, 40, or 80 μ g/mouse of either poorly-dispersed (PD) or well-dispersed (WD) NiO- and CeO₂-NP dispersed in differing dispersion medias (Panel A: pluronics, Panel B: PBS, Panel C: Survanta[®], and Panel D: DM) at 1 day post-exposure. Values are given as means \pm SE (n=8). *Significant difference of treatment group from control at 1 day post-exposure ($p < 0.05$). +Significant difference between poorly-dispersed (5 min sonication) and well-dispersed (20 min sonication) NiO- and CeO₂-NP solutions at same post-exposure timepoint ($p < 0.05$). IL-1 β concentrations were determined as described in Methods.

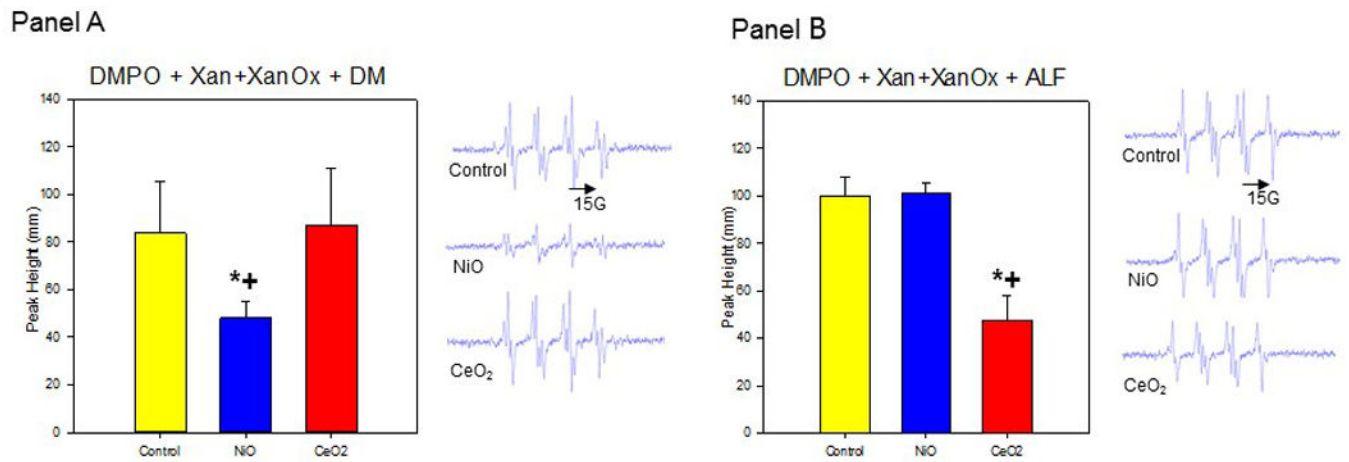


Figure 7.

Induced superoxide radicals scavenged by particles in DM. DMPO (100 mM), Xan (2U), XanOx (35 mM), and particles in DM; Centerfield 3485G; sweep width 100 G; microwave frequency 9.79 GHz; power 63 mW; time constant 40.96 ms; **Panel A (Left):** Relative peak heights of ESR spectra (n=3); **Panel A (Right):** Representative ESR spectra. Induced superoxide radicals scavenged by particles in ALF. DMPO (100 mM), Xan (2U), XanOx (35 mM), and particles in ALF; Centerfield 3485G; sweep width 100 G; microwave frequency 9.78 GHz; power 63 mW; time constant 40.96 ms; **Panel B (Left):** Relative peak heights of ESR spectra (n=3); **Panel B (Right):** Representative ESR spectra. *Significant difference between treatment group from control ($p < 0.05$). +Significant difference between CeO₂-NP and NiO-NP solutions at same post-exposure timepoint ($p < 0.05$).

Table 1

Effect of dispersion media and sonication time on average nanoparticle size (nm).

Medium Type	5 min sonication NiO	5 min sonication CeO ₂	20 min sonication NiO	20 min sonication CeO ₂
Pluronics	3060±13.5	2745±21.8	694±3.7	942±15.9
PBS	1312.5±8.4	1726±11.3	486±5.8	568±12.1
Survanta	4460.1±85.4	3530±32.7	221±6.6	261±10.9
DM	489.9±8.9	302±14.6	102±2.9	89±7.8

Dynamic light scattering (DLS) means of particle size (nm) ± standard errors (SE) are shown for each NiO/dispersion media combination and CeO₂/dispersion media combination. DLS measurements for each particle/dispersion media combination (1.6 mg/ml) were immediately performed after the specified 5 or 20 minute sonication time periods. Values presented are means of hydrodynamic diameters of particle sizes (nm) from 10 sample recordings of each nano-sized particle/dispersion media combination analyzed.

Author Manuscript

Author Manuscript

Author Manuscript

Author Manuscript

Table 2

Zeta potentials of each NiO-NP and CeO₂-NP/dispersion media combination.

Medium Type	NiO Zeta Potential (mV)	CeO ₂ Zeta Potential (mV)
Pluronics	-1.86	-1.40
PBS	-0.06	-0.29
Survanta	-0.04	-0.51
DM	-0.10	-0.31

The surface charge of the NiO-NP and CeO₂-NP in each dispersion media was analyzed using a Malvern Zetasizer Nano ZS instrument (Malvern Instruments Inc., UK). The electrophoretic mobility of the nanoparticles in each dispersion media was converted into the zeta potential by utilizing the Helmholtz-Smoluchowski equation.

Author Manuscript

Author Manuscript

Author Manuscript

Author Manuscript